Journal of Solid State Chemistry 184 (2011) 1096–1104

Contents lists available at ScienceDirect

Journal of Solid State Chemistry

journal homepage: www.elsevier.com/locate/jssc

Magnetic properties of the chemically delithiated $Li_xMn_2O_4$ with $0.07 \leq x \leq 1$

Kazuhiko Mukai [a,*], Jun Sugiyama [a], Kazuya Kamazawa [a,1], Yutaka Ikedo [a,2], Daniel Andreica [b,c], Alex Amato [b]

[a] Toyota Central Research and Development Laboratories, Inc., 41-1 Yokomichi, Nagakute, Aichi 480-1192, Japan
[b] Laboratory for Muon-Spin Spectroscopy, Paul Scherrer Institut, PSI Villigen CH-5232, Switzerland
[c] Faculty of Physics, Babes-Bolyai University, 400084 Cluj-Napoca, Romania

ARTICLE INFO

Article history:
Received 15 December 2010
Received in revised form
1 March 2011
Accepted 8 March 2011
Available online 21 March 2011

Keywords:
Lithium manganese oxide
Spinel
Magnetism
Muon spin rotation/relaxation
Lithium-ion battery

ABSTRACT

Magnetism for the $Li_xMn_2O_4$ samples with $0.07 \leq x \leq 1$, which are prepared by a chemical reaction in HNO_3 solution, is investigated by direct current susceptibility (χ) and muon-spin rotation/relaxation (μSR) measurements. The effective magnetic moment (μ_{eff}) of Mn ions decreases monotonically with decreasing x, indicating that Mn^{3+} ions with $S=2$ ($t_{2g}^3 e_g^1$) are oxidized to Mn^{4+} ions with $S=3/2$ (t_{2g}^3) with decreasing x. On the other hand, as x decreases from 1 to 0.6, the Curie–Weiss temperature (Θ_p) increases monotonically from ~ -260 to -100 K, and then levels off to -100 K with further decreasing x. This indicates that the antiferromagnetic interaction is dominant in the whole x range. For the $x=0.48$ sample, the temperature dependence of χ in field-cooling mode clearly deviates from that in zero-field-cooling mode below ~ 63 K ($=T_m$). Furthermore, the hysteresis loop is observed in the magnetization vs. field curve at 5 K. Since the zero-field μSR spectrum is well fitted by a strongly damped oscillation function, the Mn moments for the $x=0.48$ sample are in a highly disordered fashion down to the lowest temperature measured.

1. Introduction

The lithium manganese oxide spinel $Li_xMn_2O_4$ with space group $Fd\bar{3}m$, in which Li and Mn ions occupy the tetrahedral 8*a* and octahedral 16*d* sites, respectively, has been intensively studied as a positive electrode material for lithium-ion batteries [1–3]. This is due to its high operating voltage, inexpensive material cost, and low toxicity compared with $LiCoO_2$, which is currently used in commercial lithium-ion batteries. Besides an application to lithium-ion batteries, $Li_xMn_2O_4$ and related compounds have been of great interest in magnetism. In the $LiMn_2O_4$ lattice, the magnetic Mn ions are arranged at the corner of a tetrahedron (see Fig. 1(a)). More specifically, the tetrahedron is likely to consist of two Mn^{3+} ions with $S=2$ ($t_{2g}^3 e_g^1$) and two Mn^{4+} ions with $S=3/2$ (t_{2g}^3), because the average valence of the Mn ions (V_{Mn}^{ave}) is +3.5. This indicates the presence of three-dimensional geometrical frustration, if the Mn–Mn interaction is antiferromagnetic (AF). Actually, the stoichiometric $LiMn_2O_4$ exhibits an AF transition with $T_N \sim 60$ K [4–7], although its AF spin arrangement is not fully determined even by neutron scattering measurements due to the presence of a strong diffuse scattering. In addition, the fully delithiated phase $Li_0Mn_2O_4$ (λ-MnO_2), in which the V_{Mn}^{ave} should be +4, shows AF transition with $T_N=32$ K [8]. There are three different type magnetic interactions between the nearest neighboring Mn ions in $Li_xMn_2O_4$, namely, the interaction between Mn^{3+} and Mn^{3+}, Mn^{3+} and Mn^{4+}, and Mn^{4+} and Mn^{4+}. According to Goodenough–Kanamori rules [9], only a 90° superexchange Mn^{4+}–O^{2-}–Mn^{4+} coupling is ferromagnetic (FM), whereas all other couplings such as direct Mn^{3+}–Mn^{3+}, direct Mn^{4+}–Mn^{4+}, and 90° superexchange Mn^{4+}–O^{2-}–Mn^{3+}, are AF. Therefore, the AF interaction is thought to be dominant when half of the corners of the tetrahedron or all four corners of the tetrahedron are occupied by Mn^{4+} ions.

On the contrary, the spinel compounds having a superlattice structure such as $(Li_{1/2}Zn_{1/2})[Li_{1/2}Mn_{3/2}]O_4$ ($P2_13$) [10] and $Li[Mg_{1/2}Mn_{3/2}]O_4$ ($P4_332$) [11] undergo a ferromagnetic (FM) transition with $T_C=22$ and 20 K, respectively. Here, for both compounds, Li^+ (Mg^{2+}) and Mn^{4+} ions are ordered by 1:3 ratio at the regular 16*d* site of the space group $Fd\bar{3}m$ [10–12]. Since Li^+ and Mg^{2+} ions are non-magnetic, the three corners of the tetrahedron formed by four cations at the 16*d* site, are occupied by magnetic Mn^{4+} ions. The difference between $LiMn_2O_4$ (λ-MnO_2) and $Li_{1/2}Zn_{1/2}[Li_{1/2}Mn_{3/2}]O_4$ ($Li[Mg_{1/2}Mn_{3/2}]O_4$), on one hand, suggests that the occupancy of the Mn ions at the 16*d* site (z_{Mn}^{16d}) plays a significant role for determining the magnetic ground

* Corresponding author. Fax: +81 561 63 6156.
E-mail address: e1089@mosk.tytlabs.co.jp (K. Mukai).
[1] Present address: Japan Proton Accelerator Research Complex (J-PARC), 2-4 Shirakata-Shirane, Tokai, Ibaraki 319-1195, Japan.
[2] Present address: Muon Science Laboratory, Institute of Materials Structure Science, KEK, 1-1 Oho, Tsukuba, Ibaraki 305-0801, Japan.

0022-4596/$ - see front matter © 2011 Elsevier Inc. All rights reserved.
doi:10.1016/j.jssc.2011.03.019

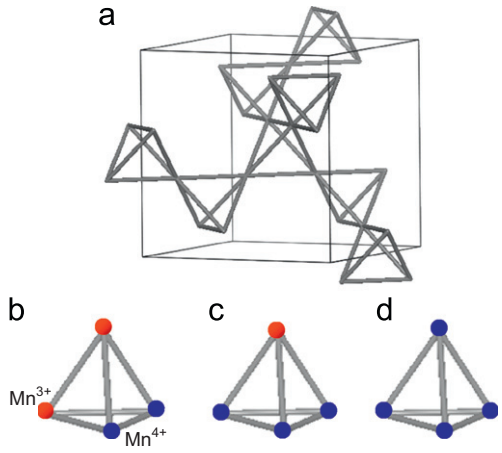

Fig. 1. (a) Schematic illustration of the crystal structure for $Li_xMn_2O_4$ having a spinel-framework structure of space group $Fd\bar{3}m$, in which Li and Mn ions sit the tetrahedral 8*a* and octahedral 16*d* sites, respectively. The magnetic Mn ions form a tetrahedron, satisfying one of the conditions for geometrical frustration. Since the average valence of the Mn ions (V_{Mn}^{ave}) is +3.5 at (b) $x=1$, the tetrahedron is likely to consist two Mn^{3+} ions (red circle) and two Mn^{4+} ions (blue circle). The amount of Mn^{4+} ions increases with decreasing x; three corners of the tetrahedron or all four corners of the tetrahedron are occupied by Mn^{4+} ions at (c) $x=1/2$ or at (d) $x=0$. Note that $Li[Mg_{1/2}Mn_{3/2}]O_4$ ($P4_332$) and $Li_{1/2}Zn_{1/2}[Li_{1/2}Mn_{3/2}]O_4$ ($P2_13$), in which three corners of the tetrahedron are occupied by Mn^{4+} ions and the rest of the corner is occupied by non-magnetic ions (Mg^{2+} or Li^+), exhibit ferromagnetic transition at $\sim T_C=20$ K. When the Mn^{3+} ions and Mn^{4+} ions at the 16*d* site are ordered by 1:1 ratio in the *Fddd* space group or ordered by 1:3 ratio in the $P4_332$ space group, the Mn^{3+} (or Mn^{4+}) ions no longer form a tetrahedron. (For interpretation of the references to color in this figure legend, the reader is referred to the web version of this article.)

state of lithium manganese oxide spinels. On the other hand, the cubic lattice parameter (a_c), i.e. the distance between the Mn ions (d_{Mn-Mn}) would also affect the magnetism on these spinels. This is because our recent magnetic susceptibility (χ) measurements on $Li_x[Ni_{1/2}Mn_{3/2}]O_4$ ($P4_332$) demonstrated that the magnetic ground state alters from FM at $x=1$ to paramagnetic (PM) or AF at $x=0.05$ with decreasing d_{Mn-Mn} from 2.882 to 2.820 Å [13,14]. Here, Ni^{2+} and Mn^{4+} ions in $Li[Ni^{2+}_{1/2}Mn^{4+}_{3/2}]O_4$ are ordered by 1:3 ratio at the regular 16*d* site of the space group $Fd\bar{3}m$ [15], as in the case for $(Li_{1/2}Zn_{1/2})[Li_{1/2}Mn_{3/2}]O_4$ ($d_{Mn-Mn}=2.887$ Å) [10] and $Li[Mg_{1/2}Mn_{3/2}]O_4$ ($d_{Mn-Mn}=2.888$ Å) [11]. Moreover, only the Ni^{2+}/Ni^{4+} redox couple is responsible for the delithiated reaction, whereas Mn^{4+} ions remain inactive [16]. Since the Ni^{4+} ions are in a non-magnetic low-spin state with t_{2g}^6 ($S=0$) [16,17], the arrangement of Mn^{4+} ions in $Li_0[Ni_{1/2}Mn_{3/2}]O_4$ is essentially the same to those in $(Li_{1/2}Zn_{1/2})[Li_{1/2}Mn_{3/2}]O_4$ and $Li[Mg_{1/2}Mn_{3/2}]O_4$. Thus, the difference in magnetism between $Li_0[Ni_{1/2}Mn_{3/2}]O_4$ and $(Li_{1/2}Zn_{1/2})[Li_{1/2}Mn_{3/2}]O_4$ (or $Li[Mg_{1/2}Mn_{3/2}]O_4$) could be explained by the dependence of magnetic interactions on d_{Mn-Mn}, if we ignore the effects on the non-magnetic Li^+ and Zn^{2+} ions at the 8*a* site [13].

During the delithiation process of $Li_xMn_2O_4$, the amount of Mn^{4+} ions at the corners of the tetrahedron increasing with decreasing x; two Mn^{4+} ions for $x=1$, three Mn^{4+} ions for $x=0.5$, and four Mn^{4+} ions for $x=0$ (Fig. 1(b)–(d)). Moreover, the value of d_{Mn-Mn} for the $x=1/2$ compound ($Li_{1/2}[Mn^{3+}_{1/2}Mn^{4+}_{3/2}]O_4$) is reported to be 2.88 Å [2], and is almost similar to those for $(Li_{1/2}Zn_{1/2})[Li_{1/2}Mn_{3/2}]O_4$ ($P2_13$) [10], $Li[Mg_{1/2}Mn_{3/2}]O_4$ ($P4_332$) [11], and $Li[Ni_{1/2}Mn_{3/2}]O_4$ ($P4_332$) [13–17]. The magnetic study on delithiated $Li_xMn_2O_4$, hence, provides crucial information on the complex magnetic properties of lithium manganese oxide spinels. However, to our knowledge, the magnetism of $Li_xMn_2O_4$ with $0<x<1$ has never been reported, except for the results of *ab initio* calculations [18]. In this paper, we report the results of χ and muon spin rotation/relaxation (μSR) measurements for the chemically delithiated $Li_xMn_2O_4$ samples with $0.07\le x\le 1$ and discuss the magnetic phase diagram for $Li_xMn_2O_4$.

2. Experimental section

A polycrystalline sample of $LiMn_2O_4$ was synthesized by a conventional solid-state reaction technique using reagent grade Li_2CO_3 and MnO_2 (Mitsui Mining & Smelting Co. Ltd., Japan) powders. The reaction mixture was heated at 900 °C for 12 h in air and then cooled down to room temperature (T) at 5 °C · min^{-1}. The obtained $LiMn_2O_4$ powder was characterized by a powder X-ray diffraction (XRD) analysis and an electrochemical charge/discharge test in a non aqueous lithium cell. XRD measurements were performed at a synchrotron radiation facility of SPring-8 (BL19B2) in the T range between 260 and 320 K. The delithiated $Li_xMn_2O_4$ sample was prepared by a chemical reaction as reported previously [1,19]. That is, 3.6 g (~0.02 mol) of $LiMn_2O_4$ powder was immersed in 100 mL HNO_3 solution and stirred for 24 h at room T. The concentration of HNO_3 (c_M) solution was 0.05, 0.1, 0.15, 0.19, 0.20, 0.225, 0.25, 0.30, 0.35, 0.375, 0.40, and 0.50 M, respectively. After the acid treatment, the sample was filtered and dried at 60 °C for 24 h. The Li/Mn ratio, i.e. x in $Li_xMn_2O_4$ was determined by an inductively coupled plasma-atomic emission spectrometer (ICP-AES, CIROS 120, Rigaku Co. Ltd., Japan). As seen in Fig. 2, x decreases almost linearly with increasing c_M up to 0.40 M, indicating that the following disproportionation reaction proceeds as expected:

$$4Li_xMn_2O_4+8H^+\rightarrow 6\lambda\text{-}MnO_2+4xLi^++2Mn^{2+}+4H_2O \quad (1)$$

The crystal structure for the $Li_xMn_2O_4$ samples was examined by powder XRD measurements with iron $K\alpha$ radiation (D8 ADVANCE, Bruker AXS, Inc.) at room T (~25 °C). In order to confirm the existence/absence of oxygen deficiency and H^+ ions in the $Li_xMn_2O_4$ sample, thermogravimetric (TG, TGA-50, Shimadzu Co. Ltd., Japan) and pyrolysis gas chromatography/mass spectroscopy (Py-GC/MS, Py-2010D, Frontier Lab Co. Ltd., Japan) analyses were performed.

χ ($=M/H$, where M is the magnetization and H is the magnetic field) was measured using a superconducting quantum interference device magnetometer (MPMS, Quantum Design) in the T range between 5 and 400 K under $H\le 55$ kOe. χ was also measured in the T range between 5 and 100 K with $H=100$ Oe in both zero-field-cooling (ZFC) and field-cooling (FC) modes. First, the sample was cooled down to 5 K in ZF from 100 K, then a magnetic field was applied, and finally χ_{ZFC} was measured with increasing T from 5 to 100 K (80 K for the $x=1$ and 0.85 samples). Subsequently, χ_{FC} was measured with decreasing T from 100 (80 for the $x=1$ and 0.85 samples) to 5 K. We also performed μSR

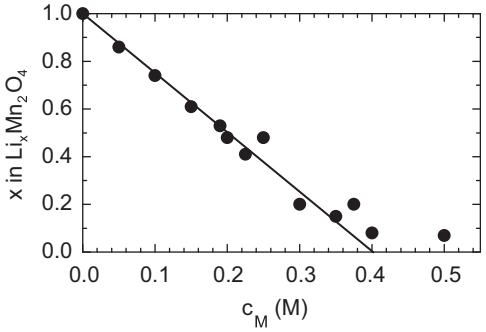

Fig. 2. The relationship between x in $Li_xMn_2O_4$ and the HNO_3 concentration (c_M) for the chemically delithiation reaction. The delithiated $Li_xMn_2O_4$ samples were prepared by adding the $LiMn_2O_4$ powder (3.6 g) to HNO_3 solution in the c_M range between 0.05 and 0.5 M. The solid line indicates the calculated Li composition based on Eq. (1).

measurements at the GPS beamline of Paul Scherrer Institut, Switzerland. The $x=0.48$ sample was pressed into a disk with 15 mm diameter and ~1 mm thickness, then the disk was packed by an aluminized Kapton foil, and finally placed in a muon-veto sample holder. The details of the experimental setup and technique are described in elsewhere [20].

3. Results

3.1. Structural and thermal analyses

Fig. 3(a) shows the XRD patterns for the $Li_xMn_2O_4$ samples with $x=1$, 0.85, 0.74, 0.48, 0.20, and 0.07. All the $Li_xMn_2O_4$ samples are identified as a spinel-framework structure with space group of $Fd\bar{3}m$, in which the tetrahedral 8*a* and octahedral 16*d* sites are occupied by lithium and manganese ions, respectively. For the samples with $1>x>0.07$, the XRD peaks are broad compared with those for the $x=1$ and 0.07 samples. Furthermore, as seen in the enlarged XRD pattern (right side of Fig. 3(a)), an additional XRD peak indicated by arrow is slightly observed in the vicinity of the major XRD peak. This indicates that the sample with $1>x>0.07$ is not a single-phase but a mixture of different cubic phases, although the average Li composition almost agrees with the calculated Li composition based on Eq. (1) (see Fig. 2).

Fig. 3(b)–(d) shows the results of a Rietvled analysis by RIETAN2000 [21] for the $x=1$, 0.48, and 0.07 samples, respectively. The structural parameters such as cubic lattice parameter (a_c), oxygen position, and isotropic atomic displacement factor (B_{iso}) are listed in Table 1. The Rietveld analysis for the samples with $1>x>0.07$ are performed under the assumption that the sample is in a mixture of two different cubic phases. As seen in Fig. 4, the a_c vs. x curve of the major phase is almost consistent with that for the electrochemically delithiated $Li_xMn_2O_4$ compounds [2], except for the $x=0.85$ and 0.74 samples. That is, as x decreases from 1 to 0.61, a_c monotonically decreases from 8.240(5) to 8.162(5) Å, and then rapidly drops to ~8.03 Å with further decreasing x.

Fig. 5 shows the results of (a) TG and (b) Py-GC/MS analyses for the $x=0.07$ sample. The TG curve exhibits two sudden decreases around 820 and 1130 K. The change in the sample weight at 1000 and 1200 K are 90.7% and 87.9%, respectively, which agree with the calculated values of the following oxygen evolution reactions:

$$MnO_2 \rightarrow 1/2Mn_2O_3 + 1/4O_2 \text{ (weight loss from } MnO_2\text{: 9.2\%)} \quad (2)$$

$$Mn_2O_3 \rightarrow 2/3Mn_3O_4 + 1/6O_2 \text{ (weight loss from } MnO_2\text{:12.3\%)} \quad (3)$$

This indicates the absence of oxygen deficiency in the bulk of the sample, although we cannot exclude the possibility of the non-stoichiometric defects on the surface. As seen in Fig. 5(b), there are two peaks centered around 840 and 1130 K in the O_2^+ (mass/charge=32) spectrum. The former corresponds to the reaction described in Eq. (2), while the latter the reaction described in Eq. (3). Two broad peaks are also observed in the H_2O^+ (mass/charge=18) spectrum. The peaks around 450 and 650 K are attributed to the dehydration reactions of absorbed/adsorbed water and structurally bonded/intercalated water, respectively. Thus, the Py-GC/MS analysis shows that H^+ ions exist in the crystal lattice of the $x=0.07$ sample, as for the chemically delithiated Li_xNiO_2, more specifically $H_{\sim 0.5}Li_{0.01}NiO_2$ [19,22]. However, the peak ratio of H_2O^+/O_2^+ for the $x=0.07$ sample is significantly small (~0.02) compared with that for $H_{\sim 0.5}Li_{0.01}NiO_2$ (~0.25). If we assume that the peak ratio of H_2O^+/O_2^+ corresponds to the amount of H^+ ions, the chemical formula for the $x=0.07$ sample is represented as $H_{\sim 0.08}Li_{0.07}Mn_2O_4$. Thus, the chemically delithiation reaction of $Li_xMn_2O_4$ is almost completed, although that of Li_xNiO_2 induced the insertion of large amount of H^+ ions in the lattice [19,22].

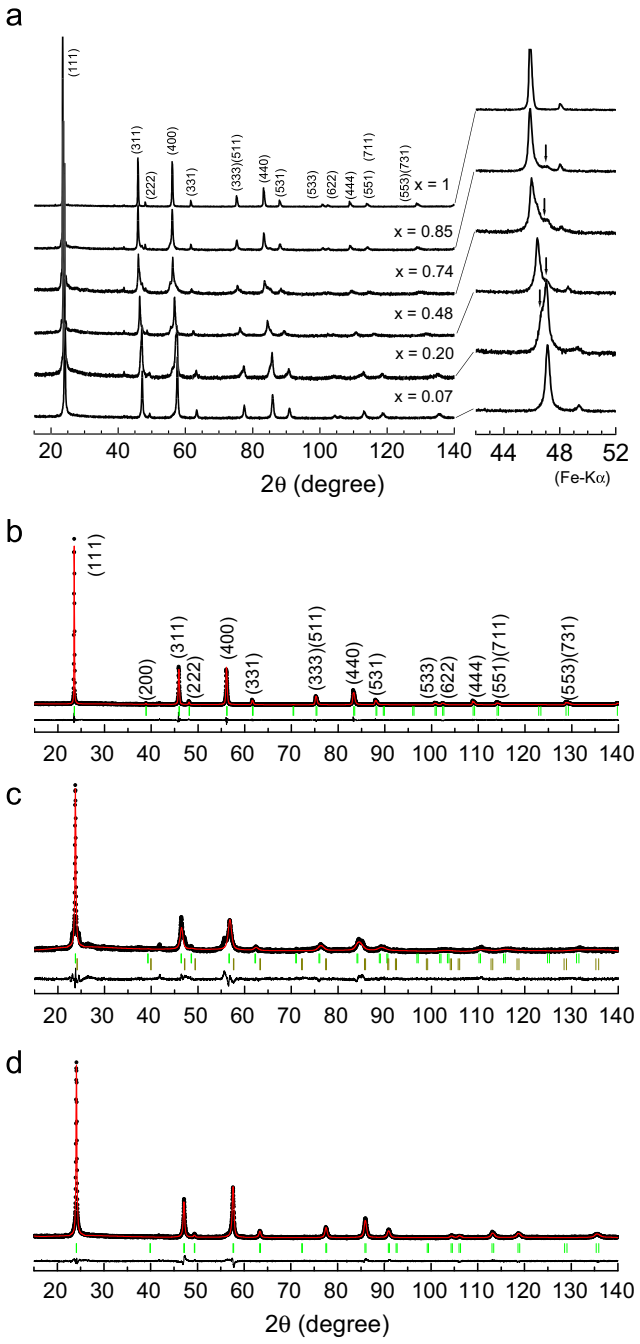

Fig. 3. (a) X-ray diffraction (XRD) patterns for the $Li_xMn_2O_4$ samples with $x=1$, 0.85, 0.74, 0.48, 0.20, and 0.07. According o the enlarged XRD patterns in the 2θ range between 42° and 52° (right side), a minor phase indicated by arrow is slightly observed for the samples with $1>x>0.07$. The results of Rietveld analyses for the (b) $x=1$, (c) 0.48, and (d) 0.07 samples are also shown. The observed (I_{obs}) and calculated (I_{calc}) intensity data are plotted as points and solid line, respectively, in the upper field. The bar-code-type indications are the Bragg reflections. The difference between I_{obs} and I_{calc} is shown in the lower field.

3.2. Macroscopic magnetism by χ

Fig. 6 shows the T dependence of (a) χ and (b) χ^{-1} for the $Li_xMn_2O_4$ samples with $x=1$, 0.85, 0.74, 0.48, 0.2, and 0.07 measured in FC mode with $H=10$ kOe. The $\chi(T)$ curves for all

Table 1
The structural parameters for the $Li_xMn_2O_4$ samples with $x=1$, 0.48, and 0.07 determined by the Rietveld analysis.

Sample	Space group	Atom	Wyckoff position	Occupancy g	x	y	z	B_{iso}/Å^2
$x=1$	$Fd\bar{3}m$	Li	8*a*	1.0	1/8	1/8	1/8	0.2(2)
		Mn	16*d*	1.0	1/2	1/2	1/2	1.1(1)
		O	32*e*	1.0	0.262(1)	0.262(1)	0.262(1)	2.7(1)
$a_c=8.2404(2)$ Å, $R_{wp}=3.06$, $R_B=2.03$, and $S=1.50$								
$x=0.48$	$Fd\bar{3}m$ (major)	Li1	8*a*	0.55	1/8	1/8	1/8	0.3(2)
		Mn1	16*d*	1.0	1/2	1/2	1/2	1.1(1)
		O1	32*e*	1.0	0.262(1)	0.262(1)	0.262(1)	1.3(1)
	$Fd\bar{3}m$ (minor)[a]	Li2	8*a*	0.1	1/8	1/8	1/8	0.3(2)
		Mn2	16*d*	1.0	1/2	1/2	1/2	1.1(1)
		O2	32*e*	1.0	0.262(1)	0.262(1)	0.262(1)	1.3(1)
$a_{c1}=8.1580(9)$ Å, $a_{c2}=8.0330(6)$ Å, $R_{wp}=3.40$, $R_B=2.06$, and $S=1.65$								
$x=0.07$	$Fd\bar{3}m$	Li	8*a*	0.07	1/8	1/8	1/8	0.5(2)
		Mn	16*d*	1.0	1/2	1/2	1/2	0.9(1)
		O	32*e*	1.0	0.261(1)	0.261(1)	0.261(1)	2.0(1)
$a_c=8.0333(4)$ Å, $R_{wp}=3.20$, $R_B=2.06$, and $S=1.55$								

[a] The weight fraction of the minor phase is about 16%.

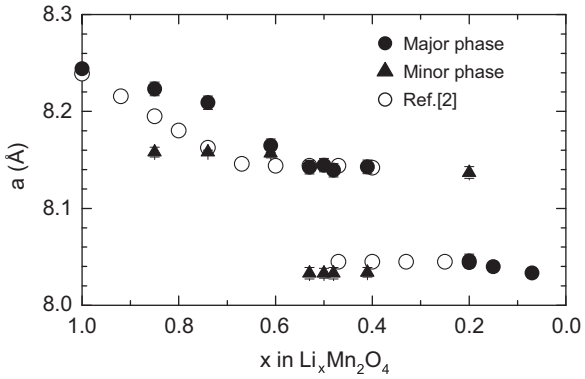

Fig. 4. Variation of cubic lattice parameter (a_c) as a function of x in $Li_xMn_2O_4$. The values of a_c for the major (closed circles) and minor (closed triangles) phases were calculated by a Rietveld analysis with RIETAN2000. The values of a_c in Ref. [2] (open circles), which were prepared by an electrochemical reaction, are also shown for comparison.

the samples show a Curie–Weiss paramagnetic behavior above ~200 K, except for a small cusp at $T_{JT}=290$ K for the $x=1$ sample due to a cooperative Jahn–Teller (JT) transition of Mn^{3+} ions with $S=2$ ($t_{2g}^3e_g^1$) [4,23]. Actually, the XRD measurements on the $x=1$ sample confirmed the structural phase transition around 290 K from the high-T cubic phase ($Fd\bar{3}m$) to low-T orthorhombic phase ($Fddd$). For the PM state, the Curie–Weiss law in the general form is written as

$$\chi = \frac{N\mu_{\mathrm{eff}}{}^2}{3k_B(T-\Theta_p)} + \chi_0 \quad (4)$$

where N is the number density of the Mn ions, μ_{eff} is the effective magnetic moment of the Mn ions, k_B is the Boltzmann's constant, T is the absolute temperature, Θ_p is the paramagnetic Curie–Weiss temperature. Using Eq. (4) in the T range between 200 and 400 K, we obtain the values of μ_{eff} and Θ_p for the $Li_xMn_2O_4$ samples. As shown in Fig. 7(a), the obtained μ_{eff} decreases monotonically with decreasing x, being consistent with the spin-only predicted value of $\mu_{\mathrm{eff}}^{\mathrm{pre}}$. Here, $\mu_{\mathrm{eff}}^{\mathrm{pre}}$ was calculated by the assumption that Mn^{3+} ions are in the high-spin state with $S=2$ ($t_{2g}^3e_g^1$), Mn^{4+} ions with $S=3/2$ (t_{2g}^3), and the gyromagnetic ratio $g=2$. The monotonic decrease in μ_{eff} with x, hence, indicates that the increase in the amount of Mn^{4+} ions is proportional to x as expected. This is very different from the case for the chemically delithiated Li_xNiO_2,

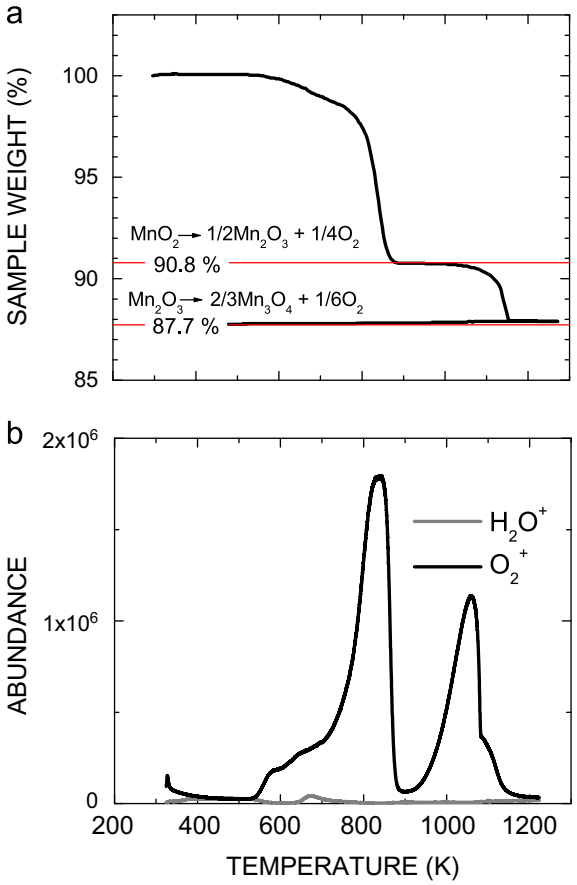

Fig. 5. (a) Thermogravimetric (TG) and (b) pyrolysis gas chromatography/mass spectroscopy (Py-GC/MS) analyses for the $Li_xMn_2O_4$ samples with $x=0.07$. Heating rates are 10 K min^{-1} for (a) and 20 K min^{-1} for (b).

because μ_{eff} ($=1.43\ \mu_B$) for the chemically delithiated Li_xNiO_2 is considerably large compared with the prediction for the spin-only value ($\mu_{\mathrm{eff}}^{\mathrm{pre}} \sim 0\ \mu_B$) due to the presence of H^+ ions [18,19]. On the other hand, the value of Θ_p for the $x=1$ sample is estimated as ~ −260 K, and is almost comparable to the past results of $\Theta_p=-337$ [4], −273 [24], and −266 K [25] (see Fig. 5(b)). As x decreases from 1 to 0.6, Θ_p increases monotonically up to ~ −100 K,

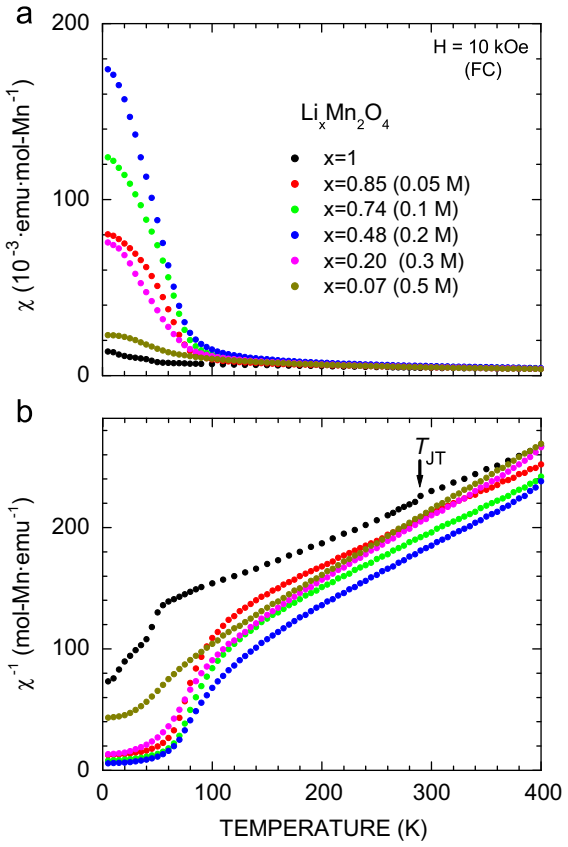

Fig. 6. Temperature dependence of the (a) magnetic susceptibility (χ) and (b) inverse magnetic susceptibility (χ^{-1}) for the $Li_xMn_2O_4$ samples with $x=1$, 0.85, 0.74, 0.48, 0.20, and 0.07 measured in field-cooling (FC) mode with $H=10$ kOe. T_{JT} is the structural phase transition temperature due to a cooperative Jahn–Teller (JT) effect of the Mn^{3+} ions with $S=2$ ($t_{2g}^3e_g^1$).

and then levels off to ~ -100 K with further decreasing x. This means that the AF interaction weakens with decreasing x, particularly in the x range below 0.6. However, the negative Θ_p value suggests that the AF interaction is dominant even for the $x<0.6$ samples.

As seen in Fig. 6(a), χ for the samples with $0.07<x<1$ increases rapidly below 100 K, indicating that ferromagnetic (FM) components appear in these samples. Furthermore, the $x=0.48$ sample exhibits the highest χ at 5 K. Here, the amount of Mn^{4+} ions at the tetrahedron for the $x=0.5$ compound ($=Li_{1/2}[Mn^{3+}_{1/2}Mn^{4+}_{3/2}]O_4$) is similar to those for $Li_{1/2}Zn_{1/2}[Li_{1/2}Mn_{3/2}]O_4$ ($P2_13$) [10], $Li[Mg_{1/2}Mn_{3/2}]O_4$ ($P4_332$) [11], and $Li[Ni_{1/2}Mn_{3/2}]O_4$ ($P4_332$) [13–17], although one corner of the tetrahedron is occupied by magnetic Mn^{3+} ions and Li^+ ions at the 8a site are partially delithiated. In addition, the d_{Mn-Mn} for the $x=0.48$ sample is calculated to be 2.884 Å by the value of $a_c(\sqrt{2}a_c/4)$, and is almost comparable to those for $Li_{1/2}Zn_{1/2}[Li_{1/2}Mn_{3/2}]O_4$ ($d_{Mn-Mn}=2.896$) [10], $Li[Mg_{1/2}Mn_{3/2}]O_4$ ($d_{Mn-Mn}=2.898$ Å) [11], and $Li[Ni_{1/2}Mn_{3/2}]O_4$ ($d_{Mn-Mn}=2.886$ Å) [13–17]. Therefore, the magnetization, χ in both ZFC and FC modes, and μSR were measured in order to clarify the magnetic ground state for the $x=0.48$ sample. Here, μSR is very sensitive to a local magnetic environment and is one of the most powerful tools to detect static magnetic order, such as FM, AF, and ferrimagnetic [19].

Fig. 8 shows the (a) magnetization (M) as a function of H at 5 K for the $Li_xMn_2O_4$ samples, (b) enlarged $M(H)$ curves, and (c) x dependence of the remanent magnetization (M_r) and the coercive field (H_c). As x decreases from 1, the net magnetic moment, i.e. M at $H=55$ kOe increases up to $x=0.48$, then decreases with

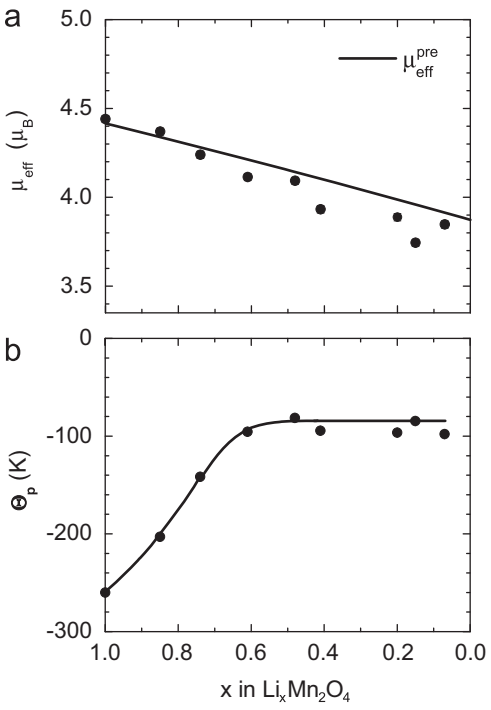

Fig. 7. x dependence of the (a) effective magnetic moment (μ_{eff}) and (b) Curie–Weiss temperature (Θ_p) for the $Li_xMn_2O_4$ samples. The solid line in (a) is the predicted effective magnetic moment (μ_{eff}^{pre}) for $Li_xMn_2O_4$ under the assumption that Mn^{3+} are in the high-spin state with $S=2$ ($t_{2g}^3e_g^1$), Mn^{4+} ions with $S=3/2$ (t_{2g}^3), and $g=2$. The negative values of Θ_p indicate that the antiferromagnetic interaction is dominant in the whole x range.

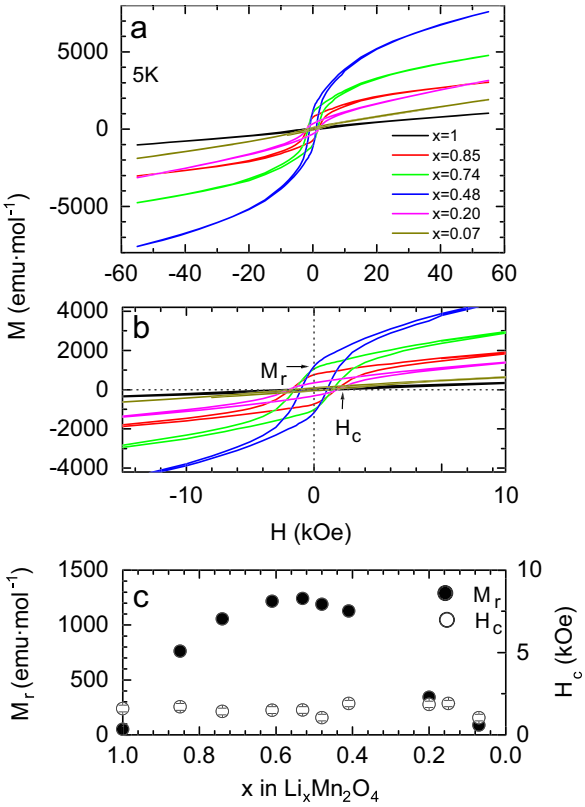

Fig. 8. (a) Magnetization (M) as a function of field (H) at 5 K for the $Li_xMn_2O_4$ samples with $x=1$, 0.85, 0.74, 0.48, 0.20, and 0.07, (b) the enlarged M vs. H curve, and (c) remanent magnetization (M_r) and coercive field (H_c) as a function of x in $Li_xMn_2O_4$.

further decreasing x. The $M(H)$ curve for the $x=0.48$ sample shows not a FM but a ferrimagnetic-like behavior. That is, as H increases from 0 kOe, M rapidly increases with changing its slope up to ~20 kOe, and then increases almost linearly with further increasing H. The magnitude of M does not level off even at $H=55$ kOe. As seen in Fig. 8(b), a hysteresis loop is clearly observed at $H \leq 10$ kOe, indicating the presence of a FM component in the $x=0.48$ sample. Although a small hysteresis loop is also observed for the $x=1$ and 0.07 samples, the x dependence of M_r shows a maximum around $x=0.5$, whereas the value of H_c is almost x-independent; $H_c \sim 1.5$ kOe (see Fig. 8(c)). This means that, as x decreases from 1, the amount of the FM component (the area of hysteresis loop) caused by the $x \sim 0.5$ phase increases up to 0.5, then decreases with further decreasing x.

Fig. 9 shows the $\chi(T)$ curves measured in both ZFC and FC modes for the $Li_xMn_2O_4$ samples with (a) $x=1$, (b) $x=0.85$, (c) $x=0.74$, (d) $x=0.61$, and (e) $x=0.53$. Fig. 10 shows those for the $Li_xMn_2O_4$ samples with (a) $x=0.48$, (b) $x=0.41$, (c) $x=0.20$, (d) $x=0.15$, and (e) $x=0.07$. The stoichiometric $LiMn_2O_4$ is known to exhibit the AF transition with $T_N=40$ K by ^{7}Li-NMR measurements [4] or $T_N=60$ K by neutron scattering measurements [5–7]. However, both $\chi_{ZFC}(T)$ and $\chi_{FC}(T)$ curves for the $x=1$ sample are different from that for a typical AF transition [9]; χ_{FC} rapidly increases with decreasing T below 55 K, probably due to a canted

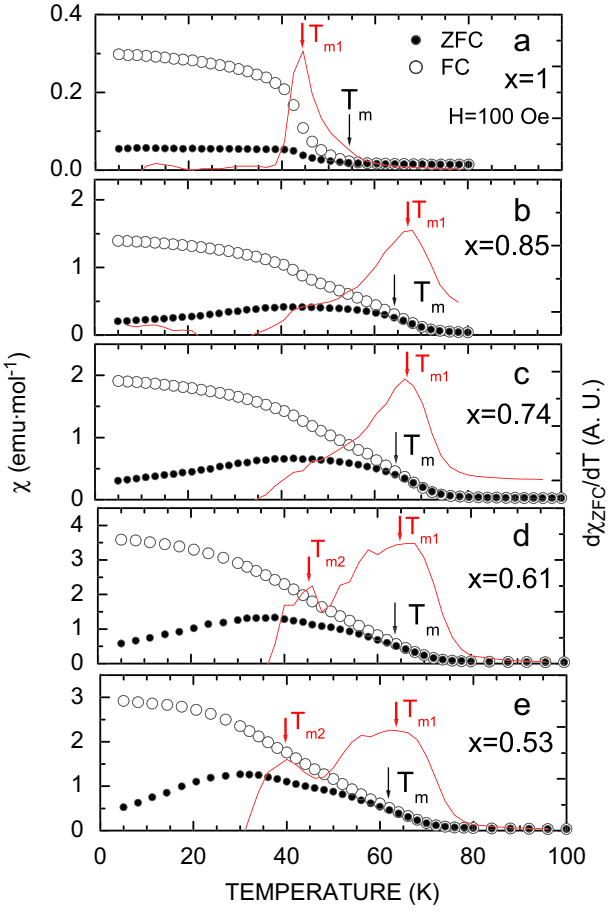

Fig. 9. Temperature dependence of the magnetic susceptibility (χ) measured in both zero-field-cooling (ZFC) and field-cooling (FC) modes with $H=100$ Oe for the $Li_xMn_2O_4$ samples with (a) $x=1$, (b) $x=0.85$, (c) $x=0.74$, (d) $x=0.61$, and (e) $x=0.53$. T_m is defined as the temperature at which the $\chi_{FC}(T)$ curve deviates from the $\chi_{ZFC}(T)$ curve. Temperature dependence of the differentiation of χ_{ZFC} ($d\chi_{ZFC}/dT$) is also shown (red line). T_{m1} and T_{m2} represent the first highest peak and second highest peak in $d\chi_{ZFC}/dT$, respectively. (For interpretation of the references to color in this figure legend, the reader is referred to the web version of this article.)

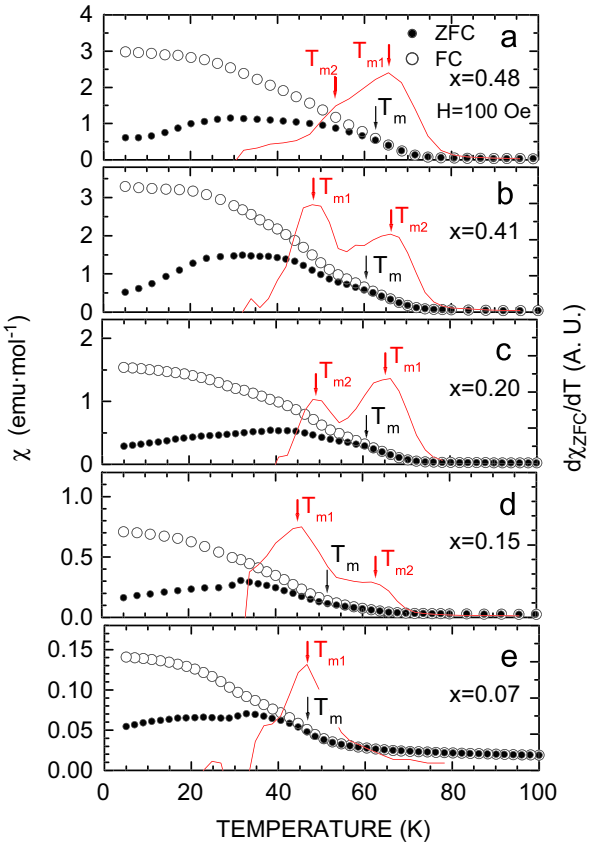

Fig. 10. Temperature dependence of the magnetic susceptibility (χ) measured in both zero-field-cooling (ZFC) and field-cooling (FC) modes with $H=100$ Oe for the $Li_xMn_2O_4$ samples with (a) $x=0.48$, (b) $x=0.41$, (c) $x=0.20$, (d) $x=0.15$, and (e) $x=0.07$. T_m is defined as the temperature at which the $\chi_{FC}(T)$ curve deviates from the $\chi_{ZFC}(T)$ curve. Temperature dependence of the differentiation of χ_{ZFC} ($d\chi_{ZFC}/dT$) is also shown (red line). T_{m1} and T_{m2} represent the first highest peak and second highest peak in $d\chi_{ZFC}/dT$, respectively. (For interpretation of the references to color in this figure legend, the reader is referred to the web version of this article.)

spin structure in the sample [5]. For the $x<1$ samples, the $\chi_{FC}(T)$ curve also deviates from the $\chi_{ZFC}(T)$ curve, suggesting the existence of a FM, ferrimagnetic, or spin-glass-like transition. Note that the transition temperature (T_m) increases with decreasing x down to 0.5, and then decreasing with further decreasing x. Here, T_m is defined as the temperature at which the $\chi_{FC}(T)$ curve deviates from the $\chi_{ZFC}(T)$ curve. Thus, $T_m=T_N=55$ K for the $x=1$ sample, while $T_m=63$ K for the $x=0.48$ sample. For the $x=0.07$ sample, the FM component is still observed in the $\chi_{FC}(T)$ curve below ~40 K, although λ-MnO_2 is reported to exhibit the AF transition at $T_N=32$ K by neutron scattering measurements [8].

3.3. Microscopic magnetism by μSR

Fig. 11(a) shows the T dependence of the ZF-μSR spectra for the $x=0.48$ sample in the time below 10 μs. The comparison in the ZF-μSR spectrum at 1.8 K ($t \leq 0.1$ μs) between the $x=0.48$ sample and $Li[Mg_{1/2}Mn_{3/2}]O_4$ ($P4_332$) [11] is also shown in Fig. 11(b). In the ZF-μSR spectrum for $Li[Mg_{1/2}Mn_{3/2}]O_4$ ($P4_332$), a first minimum at $t \sim 0.015$ μs and a second minimum at $t \sim 0.039$ μs are clearly observed, suggesting that the static magnetic order exists in the sample. Since the $M(H)$ curve exhibits a typical FM hysteresis at $H \leq 5$ kOe, $Li[Mg_{1/2}Mn_{3/2}]O_4$ ($P4_332$) enters into FM phase below $T_C=20$ K [11]. On the contrary, the ZF-μSR spectrum for the $x=0.48$ sample lacks an oscillatory signal but shows a fast relaxation in the time domain below 0.1 μs. Since the ZF-μSR spectrum at 1.8 K seems to have a first

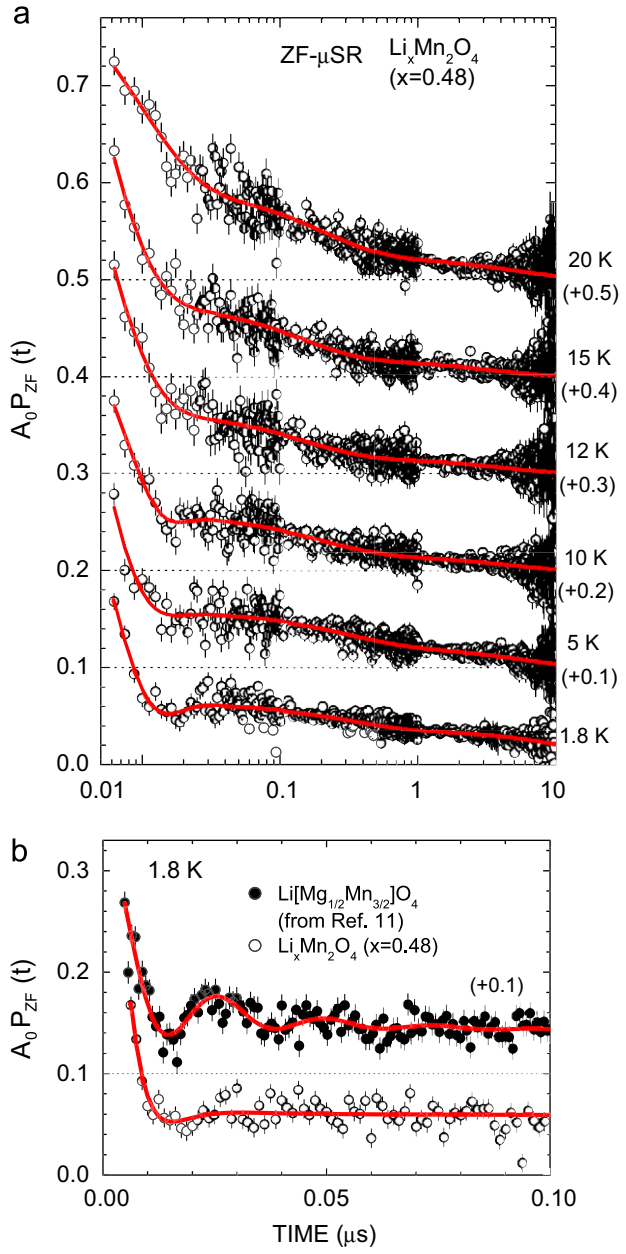

Fig. 11. (a) Temperature dependence of zero-field (ZF-) μSR spectra for the $Li_xMn_2O_4$ sample with $x=0.48$ in the time domain below 10 μs. The solid line represents the fitting result with Eq. (6). The top of five ZF-μSR spectra are shifted upward by +0.1 for clarity of display. Note that the full asymmetry (~0.24) is not obtained at $T<15$ K, because the relaxation rate is too fast for μSR. Comparison between $x=0.48$ and $Li[Mg_{1/2}Mn_{3/2}]O_4$ ($P4_332$) in ZF-μSR spectrum in the time domain below 0.1 μs is also shown in (b). The oscillatory signal in $Li[Mg_{1/2}Mn_{3/2}]O_4$ ($P4_332$) indicates the formation of static magnetic order in the sample.

minimum at around 0.017 μs, we firstly attempted to fit the ZF-μSR spectrum by a dynamic Gaussian Kubo–Toyabe [26] (DGKT) function $G_{DGKT}(t, \Delta, \nu)$, where Δ is the field distribution width, and ν is the field fluctuation (hopping) rate. When $\nu=0$, $G_{DGKT}(t, \Delta, \nu)$ is the static Gaussian Kubo–Toyabe function $G_{zz}^{KT}(t, \Delta)$ given by [26]

$$G_{zz}^{KT}(t,\Delta)=1/3+2/3(1-\Delta^2t^2)\exp\left(-\frac{\Delta^2t^2}{2}\right) \quad (5)$$

However, in order to fit the ZF-μSR spectrum in the early domain below 0.01 μs, we need additional fast exponential relaxation function, i.e. $G_{DGKT}(t, \Delta, \nu)+\exp(-\lambda_{fast}t)$ or $G_{zz}^{KT}(t, \Delta)\times\exp(-\lambda_{fast}t)$. This indicates that there are at least two muon sites in the $x=0.48$ lattice, or that the muon spins are depolarized by two different processes. According to the calculated Δ values on $Li_{0.2}[Li_{0.04}Mn_{1.96}]O_4$ [27] and $Li_{0.09}Mn_2O_4$ [28], muons are most likely to sit the vacant Li (8*a*) site in the $x=0.48$ sample. We, hence, fitted the ZF-μSR spectrum by a combination of a strongly damped oscillation signal and two exponential relaxation functions

$$A_0P_{ZF}(t)=A_1\exp(-\lambda_1t)\cos(\omega_1t+\varphi_1)+A_2\exp(-\lambda_2t)+A_3\exp(-\lambda_3t) \quad (6)$$

where A_0 is the initial asymmetry, A_i ($i=1$, 2, and 3) is the asymmetries of the three signals, λ_i is their relaxation rates, ω_1 is the Larmor frequency due to the internal field at the muon site, and φ_1 is the initial phase of the oscillatory signal.

Fig. 12 shows the T dependence of the (a) normalized asymmetries (A_i/A_0 with $i=1$, 2, and 3), (b) oscillation frequency f_1 ($=\omega_1/2\pi$), and (c) relaxation rates λ_i associated with the A_i signal.

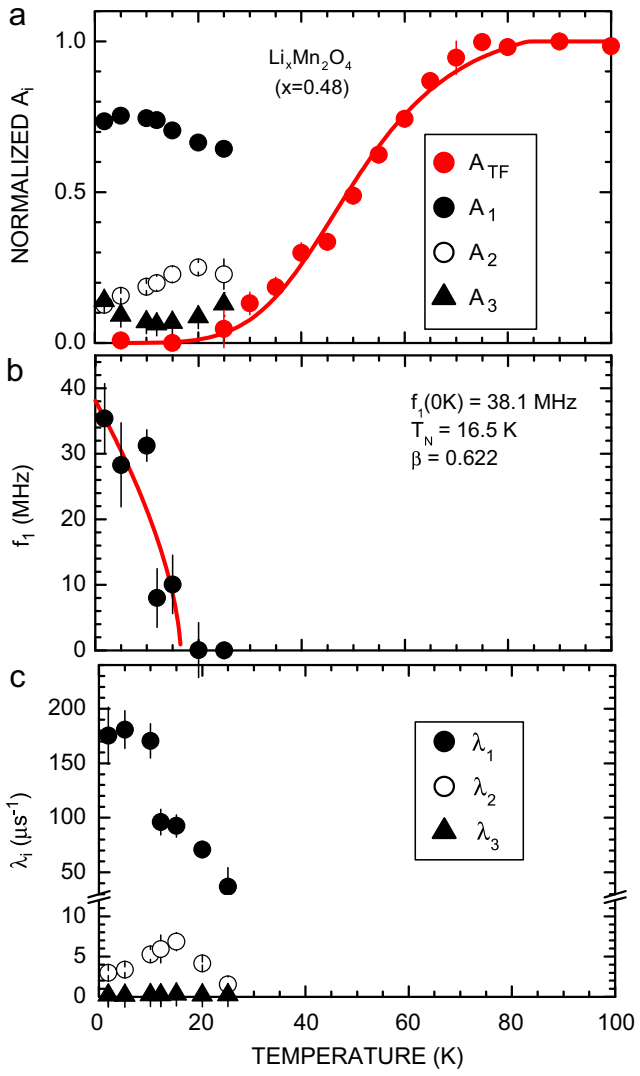

Fig. 12. Fitting results of the weak-transverse-field (wTF-) and zero-field (ZF-) μSR measurements for the $Li_xMn_2O_4$ sample with $x=0.48$: (a) normalized asymmetries of A_{TF}, A_1, A_2, and A_3, (b) oscillation frequency f_1 ($=\omega_1/2\pi$), and (c) relaxation rate λ_i associated with the A_i signal. wTF-μSR measurements were performed in the applied field with $H_{wTF}=50$ Oe. The value of A_{TF} corresponds to the volume fraction of the paramagnetic phases in the sample. The solid line in (b) is the fitting result by the function $f_1=f_1(0\text{ K})[(T_N-T)/T_N]^{\beta}$. The internal magnetic field (H_{int}) is, thus, calculated to be 2810 Oe using the muonic gyromagnetic ratio ($f_1(0\text{ K})/\gamma_\mu=38.1/13.553\times10^3$).

As T decreases from 25 K, A_1 slightly increases down to 15 K, and then keeps almost constant value ($\sim$0.74) with further lowering T. On the other hand, both f_1 and λ_1 rapidly increase with decreasing T. Although cosine oscillation function is widely used for fitting the ZF-μSR spectrum in magnetic ordered state, the value of λ_1 reaches $\sim$170 μs^{-1} at 1.8 K. This indicates that the x=0.48 sample is in a highly disordered fashion. Here, the value of A_1 is almost close to 2/3. In addition, λ_2 and λ_3 are very smaller than λ_1. Thus, both A_2 and A_3 signals are most likely to be the "1/3 tail" signal. Note that the normalized weak-transverse-field (wTF-) asymmetry A_{TF}, which corresponds to the volume fraction of the PM phases in the sample, reaches 0 below $\sim$20 K (see Fig. 12(a)). This indicates that the whole sample enters into a magnetic phase below 20 K.

4. Discussion

As seen in Fig. 7(a), the $\mu_{eff}(x)$ curve supports that the Mn^{3+} ions with S=2 ($t_{2g}^3 e_g^1$) are oxidized to the Mn^{4+} ions with S=3/2 (t_{2g}^3) with decreasing x in $Li_xMn_2O_4$. This means that the amount of Mn^{4+} ions at the corners of the tetrahedron increases with decreasing x as expected. Furthermore, since the $\chi_{FC}(T)$ curve deviates from the $\chi_{ZFC}(T)$ curve below T_m ($\leq$63 K) for all the samples measured, they are found to undergo a magnetic phase below T_m. The ZF-μSR spectrum for the x=0.48 sample is found to be heavily damped even at 1.8 K. This indicates that the x=0.48 sample is in a magnetic disordered phase even at 1.8 K. Otherwise, even if the static magnetic order exists in the x=0.48 sample, it is unlikely long range but likely short range, although μSR provides no information on the length of magnetic order.

In spite of the several neutron scattering measurements on $LiMn_2O_4$ [5–7], its ordered moments are still unknown, whereas the ordered moment for $Li_0Mn_2O_4$ (λ-MnO_2) is reported to be 2.78(9) μ_B/Mn^{4+}, which is very close to the expected saturation moment (3 μ_B) [8]. If we assume that the ordered moment for the x=0.48 sample is comparable to the value of 3.25 μ_B [$=(g\times S_{Mn3+}\times 1/2+g\times S_{Mn4+}\times 3/2)\times 1/2$] and that muons are located at the vacant 8a (Li) site, the internal magnetic field (H_{int}) is estimated to be 795 Oe by a simple dipolar calculation. Note that this estimation is the upper limit of H_{int}. On the contrary, the observed H_{int} is calculated to be 2810 Oe using the value of f_1(0 K) (=38.1 MHz) and the muonic gyromagnetic ratio ($\gamma_\mu/2\pi$= 13.553 kHz/Oe). As seen in Fig. 11(a), the ZF-μSR spectrum for the x=0.48 sample exhibits a strongly damped oscillation even at 1.8 K. The wide field distribution of H_{int} would affect the large discrepancy between the calculated and experimental H_{int} values. The other contribution would come from the distance between the muon site and Mn ions.

Fig. 13 shows the schematic magnetic phase diagram for $Li_xMn_2O_4$ determined by χ and μSR measurements. Considering the past neutron results on $LiMn_2O_4$ [5–7] and $Li_0Mn_2O_4$ [8], one can argue that there are three distinct phases in the phase diagram of $Li_xMn_2O_4$; namely, the AF ordered phase with T_N=60 K for $LiMn_2O_4$, a disordered magnetic phase with T_m=63 K for $Li_{\sim 0.5}Mn_2O_4$, and the other AF ordered phase with T_N=32 K for $Li_0Mn_2O_4$. The samples with $1>x>\sim 0.5$ are most likely to be a mixture between $LiMn_2O_4$ and $Li_{\sim 0.5}Mn_2O_4$, while those with $\sim 0.5\geq x>0$ are a mixture between $Li_{\sim 0.5}Mn_2O_4$ and $Li_0Mn_2O_4$. This is because there are at least two peaks consisting of the first highest peak ($=T_{m1}$) and second highest peak ($=T_{m2}$) in the $d\chi_{ZFC}/dT(T)$ curve for the samples with $1>x>0$ (Figs. 9 and 10). T_{m2} for the samples with $1>x\geq 0.53$ almost corresponds to the AF transition ($=T_{m1}$) of the x=1 phase, while T_{m2} for the samples with $0.48\geq x>0$ (T_{m1} for the x=0.41 and 0.15 samples) is attributed to the AF transition ($=T_{m1}$) of the x=0 phase. As seen in Fig. 3(a), this scenario is consistent with the results of XRD measurements at room T for the samples with $1>x>0.07$. Furthermore, wTF-μSR measurements on the x=0.48 sample also supports that the sample is magnetically inhomogeneous in a microscopic scale, because the T dependence of A_{TF} shows a large transition width ($\Delta T\sim$60 K) as in the case for $Li[Li_{1/3}Mn_{5/3}]O_4$ [29] (see Fig. 12(a)). However, both μ_{eff} and Θ_p, which were estimated from the data above 200 K, change linearly with x in the x range between 1 and 0.6 (Fig. 7(a) and (b)). This implies that the contribution of the minor phase in the sample is negligibly small and that a possible T-induced phase separation occurs at a certain temperature below 200 K for the samples with $1>x\geq 0.6$. In order to confirm the above hypothesis, structural analyses especially below 60 K are crucial for $Li_xMn_2O_4$.

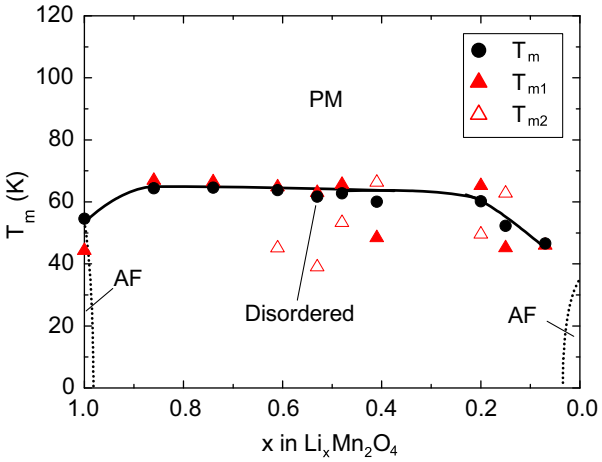

Fig. 13. Magnetic phase diagram for $Li_xMn_2O_4$ determined by magnetic susceptibility (χ) measurements and muon spin rotation/relaxation (μSR) measurements. The magnetic transition temperatures of T_m, T_{m1}, and T_{m2} are obtained by the temperature dependence of χ measured in both zero-field-cooling (ZFC) and field-cooling (FC) modes with H=100 Oe. PM and AF stand for paramagnetism and antiferromagnetism, respectively. μSR measurements indicate that the Mn moments for the x=0.48 sample are in a highly disordered fashion even at 1.8 K. The samples with $1>x>\sim 0.5$ are most likely to be a mixture between the $LiMn_2O_4$ and $Li_{\sim 0.5}Mn_2O_4$ phases, while those with $\sim 0.5\geq x>0$ are a mixture between the $Li_{\sim 0.5}Mn_2O_4$ and $Li_0Mn_2O_4$ phases. The combination of neutron scattering/heat capacity/μSR measurements would be crucial to elucidate the whole magnetic nature of $Li_xMn_2O_4$.

The spinel compounds such as $Li_{1/2}Zn_{1/2}[Li_{1/2}Mn_{1/2}]O_4$ ($P2_13$) [10] and $Li[Mg_{1/2}Mn_{3/2}]O_4$ ($P4_332$) [11] show FM order below T_C=22 and 20 K, respectively. Furthermore, $Li[Ni_{1/2}Mn_{3/2}]O_4$ ($P4_332$) exhibits ferrimagnetic order below T_C=130 K; i.e. the spin arrangements of both Ni^{2+}–Ni^{2+} and Mn^{4+}–Mn^{4+} ions are FM, while that of Ni^{2+}–Mn^{4+} is AF [12–14]. As seen in Fig. 8(a), the magnitude of M for the x=0.48 sample at 5 K is not saturated even at H=55 kOe ($\sim$7600 emu mol^{-1}). Moreover, ZF-μSR spectrum confirmed that the ground state of the x=0.48 sample is in a disordered magnetism. The existence/absence of the ordering of Mn^{3+}/Mn^{4+} ions in $Li_{0.5}Mn_2O_4$ is currently unknown at low T due to the lack of structural data below 200 K. However, the spinel compounds which show FM order have superlattice structure even at room T [10–12]. Since the d_{Mn-Mn} for the x=0.48 sample is almost comparable to that for $Li[Ni_{1/2}Mn_{3/2}]O_4$ ($P4_332$) [12–17], the distribution of Mn^{4+} ions at the 16d site, in other words superlattice structure is found to strongly correlate with the FM order for the $LiM_{1/2}Mn_{3/2}O_4$ compounds with M=Mg^{2+}, Zn^{2+}, and Ni^{2+}. Other scenario would come from the Li^+ ions at the 8a site, because the x=0.48 sample is partially delithiated.

It should be noted that the magnetic phase diagram for $Li_xMn_2O_4$ is very different from that for $Li[Li_yMn_{2-y}]O_4$. That is, as y increases from 0, not the AF transition but a spin-glass-like

transition T_f rapidly drops to $\sim$25 K even at $y \leq 0.05$, and then decreases almost linearly with further increasing y [24,30]. Here, the excess Li ions at the 16*d* site (y) in $Li[Li_yMn_{2-y}]O_4$ not only dilute the magnetic interaction but also increase the V_{Mn}^{ave}. Moreover, the value of a_c for $Li[Li_yMn_{2-y}]O_4$ decreases with increasing y [3]. Therefore, it is most likely that the dilution effect of the Li ions at the 16*d*, that is, z_{Mn}^{16d} significantly plays an important role for determining the magnetic phase diagram $Li[Li_yMn_{2-y}]O_4$. It is also interesting to note the difference in μ_{eff} between $Li_xMn_2O_4$ and $Li[Li_yMn_{2-y}]O_4$. In contrast to $Li_xMn_2O_4$, μ_{eff} for the $Li[Li_yMn_{2-y}]O_4$ compounds is significantly lower ($\sim$0.5 μ_B) than μ_{eff}^{pre} especially at $y \geq 0.05$ [24,25], although its origin is currently unknown.

Finally, we wish to discuss the effect of Li mobility on the magnetism for $Li_xMn_2O_4$. In Li_xCoO_2, one of the dynamic Kubo–Toyabe parameters Δ, which is obtained by fitting the ZF-μSR spectrum in a PM state, rapidly drops around 150 K [31]. Since ^{7}Li-NMR experiment on Li_xCoO_2 shows a step-like decrease in the NMR line width around 150 K [32], the change in Δ is caused by motional narrowing due to Li^+ diffusion [31]. On the contrary, the T dependence of Δ exhibits a rapid decrease around 250 K for $LiMn_2O_4$ [28] and 230 K for $Li_x[Li_{0.04}Mn_{1.96}]O_4$ with $x=1$ and 0.2 [27]. Although ^{7}Li-NMR and/or μSR data above 200 K is currently unavailable for $Li_xMn_2O_4$, above μSR results indicates that the Li^+ ions in the $Li_xMn_2O_4$ lattice are static below 200 K.

5. Conclusion

We have examined the magnetic nature for the $Li_xMn_2O_4$ samples by magnetic susceptibility (χ) and muon-spin rotation/relaxation (μSR) measurements. It is clarified that $Li_{\sim 0.5}Mn_2O_4$ enters into a disordered magnetic phase below $\sim$63 K. Therefore, there are three distinct phases in the magnetic phase diagram of $Li_xMn_2O_4$; the AF ordered phase with $T_N=60$ K for $LiMn_2O_4$, a disordered magnetic phase with $T_m=63$ K for $Li_{\sim 0.5}Mn_2O_4$, and the other AF ordered phase with $T_N=32$ K for $Li_0Mn_2O_4$. In order to elucidate the magnetic nature of $Li_xMn_2O_4$, it is necessary to perform neutron scattering/heat capacity/μSR measurements at low temperatures. This is because χ measurements below 60 K indicate that two sets of magnetic phase region exist in $1 > x > \sim 0.5$ and $\sim 0.5 > x > 0$, whereas x dependences of μ_{eff} and Θ_p change linearly with x in $1 \geq x \geq 0.6$. Furthermore, we expect that χ and μSR measurements for the delithiated $Li_x[Li_yMn_{2-y}]O_4$ samples provide crucial information on complex magnetic properties of lithium manganese oxide spinels. Such experiments are still in progress in our research group.

Acknowledgments

We appreciate Prof. T. Ohzuku and Dr. K. Ariyoshi of Osaka City University for preparation of $Li_xMn_2O_4$. We also thank Mr. Y. Kondo of TCRDL for ICP-AES analysis, Mr. M. Yamamoto of TCRDL for Py-GC/MAS analysis, and Prof. E. J. Ansaldo of University of Saskatchewan for helpful discussions. XRD measurements were made at the SPring-8 with the approval of the Japan Synchrotron Radiation Research Institute (Proposal No. 2007A1917). μSR measurements were done at the Swiss Muon Source, Paul Scherrer Institut (PSI), Villigen, Switzerland. We wish to thank the staff of SPring-8 and PSI for help with the experiments. This work is partially supported by Grant-in Aid for Scientific Research (B), No. 19340107 provided by MEXT, Japan. DA acknowledges financial support from the Romanian CNCSIS-UEFISCU project PNII-IDEI 2597/2009 (Contract #444).

Appendix A. Supplementary Materials

Supplementary data associated with this article can be found in the online version at doi:10.1016/j.jssc.2011.03.019.

References

[1] J.C. Hunter, J. Solid State Chem. 39 (1981) 142–147.
[2] T. Ohzuku, M. Kitagawa, T. Hirai, J. Electrochem. Soc. 137 (1990) 769–775.
[3] G. Amatucci, J.-M. Tarascon, J. Electrochem. Soc. 149 (2002) K31–K46.
[4] J. Sugiyama, T. Hioki, S. Noda, M. Kontani, J. Phys. Soc. Jpn. 66 (1997) 1187–1194.
[5] A.S. Wills, N.P. Raju, J.E. Greedan, Chem. Mater. 11 (1999) 1510–1518.
[6] I. Tomeno, Y. Kasuya, Y. Tsunoda, Phys. Rev. B 64 (2001) 094422.
[7] J.E. Greedan, C.R. Wiebe, A.S. Wills, J. Stewart, Phys. Rev. B 65 (2002) 184424.
[8] J.E. Greedan, N.P. Raju, A.S. Wills, C. Morin, S.M. Shaw, J.N. Reimers, Chem. Mater. 10 (1998) 3058–3067.
[9] J.B. Goodenough, Magnetism and the Chemical Bond, Wiley, New York, 1963.
[10] R. Plumier, M. Sougi, J. Appl. Phys. 67 (1990) 4787–4789.
[11] K. Mukai, J. Sugiyama, Y. Ikedo, P.L. Russo, J.H. Brewer, E.J. Ansaldo, K.H. Chow, K. Ariyoshi, T. Ohzuku, Physica B 404 (2009) 656–659.
[12] G. Blasse, J. Phys. Chem. Solids 27 (1966) 383–389.
[13] K. Mukai, J. Sugiyama, Solid State Commun. 150 (2010) 906–909.
[14] K. Mukai, J. Sugiyama, J. Electrochem. Soc. 157 (2010) A672–A676.
[15] Q. Zhong, A. Bonakdarpour, M. Zhang, Y. Gao, J.R. Dahn, J. Electrochem. Soc. 144 (1997) 205–213.
[16] Y. Terada, K. Yasaka, F. Nishikawa, T. Konishi, M. Yoshio, I. Nakai, J. Solid State Chem. 156 (2001) 286–291.
[17] K. Ariyoshi, Y. Iwakoshi, N. Nakayama, T. Ohzuku, J. Electrochem. Soc. 151 (2004) A296–A303.
[18] G.E. Grechnev, R. Ahuja, B. Johansson, O. Eriksson, Phys. Rev. B 65 (2002) 174408.
[19] K. Mukai, J. Sugiyama, Chem. Lett. 38 (2009) 944–945.
[20] A. Schenck, Muon Spin Rotation Spectroscopy Principles and Applications in Solid State Physics, Adam Hilger, Bristol and Boston, 1985.
[21] F. Izumi, T. Ikeda, Mater. Sci. Forum 198 (2000) 321–324.
[22] K. Mukai, J. Sugiyama, Y. Ikedo, Y. Aoki, D. Andreica, A. Amato, J. Phys. Chem. C 114 (2010) 8626–8632.
[23] J. Rodriguez-Carvajal, G. Rousse, C. Masquelier, M. Hervieu, Phys. Rev. Lett. 81 (1998) 4660–4663.
[24] P. Endres, B. Fuchs, S. Kemmler-Sack, K. Brandt, G. Faust-Becker, H.-W. Praas, Solid State Ionics 89 (1996) 221–231.
[25] C. Masquelier, M. Tabuchi, K. Ado, R. Kanno, Y. Kobayashi, Y. Maki, O. Nakamura, J.B. Goodenough, J. Solid State Chem. 123 (1996) 255–266.
[26] R.S. Hayano, Y.J. Uemura, J. Imazato, N. Nishida, T. Yamazaki, R. Kubo, Phys. Rev. B 20 (1979) 850–859.
[27] C.T. Kaiser, V.W.J. Verhoeven, P.C.M. Gubbens, F.M. Mulder, I. de Schepper, A. Yaouanc, P. Dalmas de Réotier, S.P. Cottrell, E.M. Kelder, J. Schoonman, Phys. Rev. B 62 (2000) R9236.
[28] M.J. Ariza, D.J. Jones, J. Rozière, J.S. Lord, D. Ravot, J. Phys. Chem. B 107 (2003) 6003–6011.
[29] K. Mukai, J. Sugiyama, Y. Ikedo, H. Nozaki, K. Kamazawa, D. Andreica, A. Amato, M. Månsson, J.H. Brewer, E.J. Ansaldo, K.H. Chow, J. Phys. Chem. C 114 (2010) 11320–11327.
[30] J. Sugiyama, K. Mukai, Y. Ikedo, P.L. Russo, T. Suzuki, I. Watanabe, J.H. Brewer, E.J. Ansaldo, K.H. Chow, K. Ariyoshi, T. Ohzuku, Phys. Rev. B 75 (2007) 174424.
[31] J. Sugiyama, K. Mukai, Y. Ikedo, H. Nozaki, M. Månsson, I. Watanabe, Phys. Rev. Lett. 103 (2009) 147601.
[32] K. Nakamura, H. Ohno, K. Okamura, Y. Michihiro, T. Moriga, I. Nakabayashi, T. Kanashiro, Solid State Ionics 177 (2006) 821–826.